International Symposium
On Turbulence and Shear Flow
Phenomena (TSFP-8)
August 28 - 30, 2013 Poitiers, France

DIRECT NUMERICAL SIMULATION AND MODELING OF A TURBULENT BOUNDARY LAYER WITH SEPARATION AND REATTACHMENT

Hiroyuki Abe, Yasuhiro Mizobuchi, Yuichi Matsuo
Japan Aerospace Exploration Agency
Chofu, Tokyo 182-8522, Japan
habe@chofu.jaxa.jp

Philippe R. Spalart
Boeing Commercial Airplanes
P.O. Box 3707, Seattle, WA 98124, USA
philippe.r.spalart@boeing.com

ABSTRACT

Direct numerical simulations (DNSs) of a flat-plate turbulent boundary layer with separation and reattachment have been carried out over a range of Reynolds numbers. The strong blowing and suction are imposed at the upper boundary for producing a large turbulent separation bubble, thus dealing with massive separation. The inlet data prescribed are those from DNSs of a zero-pressure-gradient turbulent boundary layer. Three values of the Reynolds number based on the freestream velocity and inlet momentum thickness (viz., 300, 600 and 983) are used. Particular attention is given to Reynolds number dependence in the bubble, streamline curvature effects and similarity to a mixing layer. Also made is an evaluation of the Reynolds-averaged Navier-Stokes (RANS) turbulence models such as k-ε, k-ω and SST models using the resulting DNS data.

INTRODUCTION

Separation of a turbulent boundary layer is encountered in engineering applications such as airfoils, diffusers and turbomachinery, where adverse pressure gradient retards a turbulent boundary layer and eventually leads to separation. This phenomenon degrades the efficiency of such devices due to the increased drag. The understanding and prediction are however still not satisfactory. The reasons may include a shortage of reliable data from numerical simulations, which account for Reynolds number dependence systematically.

DNS yields accurate and detailed turbulence quantities, thus allowing us to analyze underlying physics in a realistic manner and also to calibrate turbulence models for RANS and large eddy simulation (LES) more completely than experiments. A large amount of DNS databases have been established in canonical flows (i.e., homogeneous, channel, pipe and boundary layer) so far, where significant attention is given to Re effects. For separated flows, there is however still limited information available from DNS due perhaps to difficulties associated with inflow, boundary conditions and domain size. In particular, unlike for separation forced by the configuration (e.g., a backward facing step), there are only a few DNS attempts made for pressure-induced separation in a flat-plate turbulent boundary layer.

For the latter DNS, seminal studies were carried out by Spalart and Coleman (1997) and Na and Moin (1998) with inflow of a zero-pressure-gradient turbulent boundary layer at Reynolds number $Re_\theta \equiv U_\infty \theta_0/\nu = 300$ (U_∞ and θ_0 denote the freestream velocity and inlet momentum thickness, respectively, and ν is the kinematic viscosity) where the former and latter DNSs dealt with incipient and massive separation, respectively. Later, Skote and Henningson (2002) achieved the DNS at Re_θ=300 but with a large recirculation region. Manhart and Friedrich (2002) performed the DNS at a higher Reynolds number Re_θ=870. However, the Re dependence of the mean and turbulence quantities together with turbulence structure has yet to be examined.

In the present study, we perform the DNSs with a large separation bubble. The inlet Reynolds number Re_θ is equal to 300, 600 and 983, the latter value being about three times larger than that in the seminal DNS works, but still only about half of that in the Simpson (1989) experiment. The objectives of the present study are to quantify Reynolds number dependence in a turbulent separation bubble. Effects of streamline curvature and similarity to a mixing layer are also examined. Note that the present Re range still does not overlap with that in the Song and Eaton (2004) experiment (Re_θ=1100 ~ 20100), which also focused on the Reynolds number effects in a smoothly contoured ramp; low Reynolds number effects (Purtell et al. 1981) cannot be dismissed when interpreting the current DNS results, but the range is quite wide.

In addition, attention is given to the evaluation of two-equation turbulence models (i.e., k-ε (Abe et al. 1994), k-ω (Wilcox 1988) and SST (Menter 1994)) using the DNS data. It is hoped that, although in separated flows different performance is obtained for different geometries (see the recent review by Leschziner 2006), the present testing may provide further insight into such model performance and hence be useful for developing turbulence models for separated flows.

Table 1. Domain size, grid points and spatial resolution.

Re_θ	300	600	983
$L_x \times L_y \times L_z$	$400\theta_0 \times 120\theta_0 \times 160\theta_0$	$400\theta_0 \times 120\theta_0 \times 160\theta_0$	$366\theta_0 \times 110\theta_0 \times 146\theta_0$
$N_x \times N_y \times N_z$	$512 \times 320 \times 512$	$1024 \times 640 \times 1024$	$2048 \times 960 \times 1536$
Δx_0^+, Δy_0^+, Δz_0^+	12.4, 0.13 – 16.7, 4.95	11.5, 0.12 – 15.5, 4.59	7.97, 0.11 – 14.4, 4.25

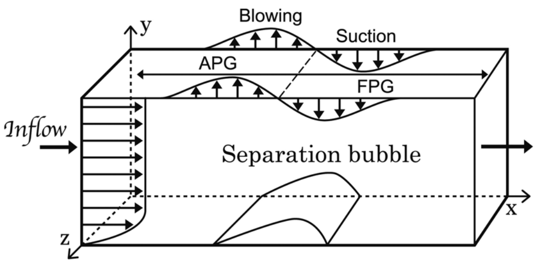

Figure 1. Computational domain.

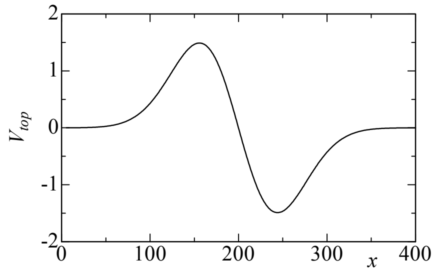

Figure 2. Transpiration velocity profile.

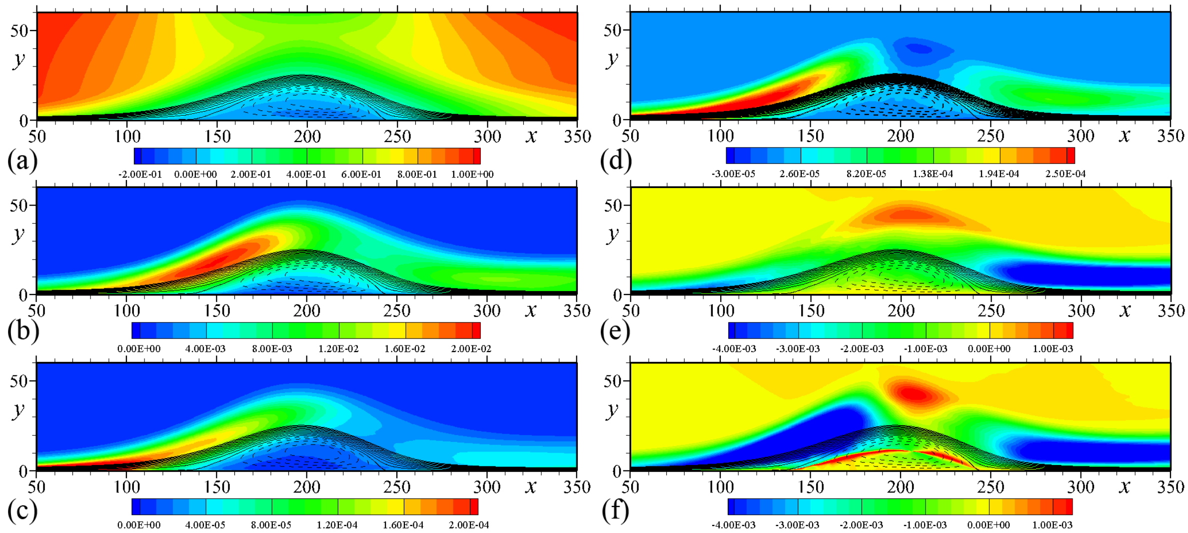

Figure 3. Distributions of mean and turbulence statistics at Re_θ=300: (a) $\bar{U}$; (b) k ; (c) ε ; (d) P_k; (e) $\overline{u_1 u_2}$; (f) $\overline{ab}$. Solid and dashed lines denote positive and negative streamlines.

NUMERICAL METHOGOLOGY

The computational domain is given in Fig. 1 where x, y and z are the streamwise, wall-normal and spanwise directions, respectively. Note that throughout the paper, all variables are normalized by U_∞ and θ_0 unless otherwise stated. The inflow data prescribed are DNS data of a zero-pressure gradient turbulent boundary layer generated by the rescaling-recycling method (Lund et al. 1998). Three values of Re_θ (=300, 600 and 983) are used. The corresponding Re_τ $(\equiv U_\tau \delta_{99} / \nu)$ is equal to 139, 255 and 360 (U_τ and δ_{99} denote the friction velocity and 99% boundary layer thickness). The transpiration profile is given in Fig. 2 where the magnitude of blowing and suction V_{top} is about three times larger (but imposed on a higher line, which compensates) than that of Spalart and Coleman (1997) to have massive separation.

Numerical methodology is briefly as follows. The current DNS code has been developed based on the channel DNS code (Abe et al. 2004). A fractional step method is used with semi-implicit time advancement. The Crank-Nicolson method is used for the viscous terms in the y direction, and the 3rd-order Runge-Kutta method is used for the other terms. A finite difference method is used as a spatial discretization. A 4th-order central scheme (Morinishi et al. 1998) is used in the x and z directions, whilst a 2nd-order central scheme is used in the y direction. The computational domain size ($L_x \times L_y \times L_z$), number of grid points ($N_x \times N_y \times N_z$) and spatial resolution at the inlet (Δx_0, Δy_0, Δz_0) are given in Table 1 where the superscript + denotes normalization by wall units. The present study uses a relatively large spanwise domain to prevent artificial constraint to large-scale structures existing in the separated shear layer and recovery region. Note also that the domain size for Re_θ=983 is about 8 percent smaller than that for Re_θ=300 and 600 so that in the subsequent plots, the x location for Re_θ=983 is adjusted to have the same V_{top}=0 location as for Re_θ=300 and 600.

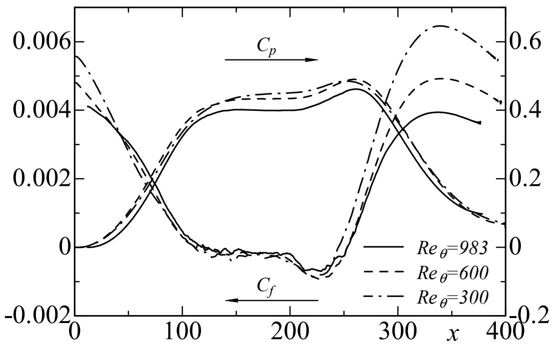

Figure 4. Distributions of C_f and C_p.

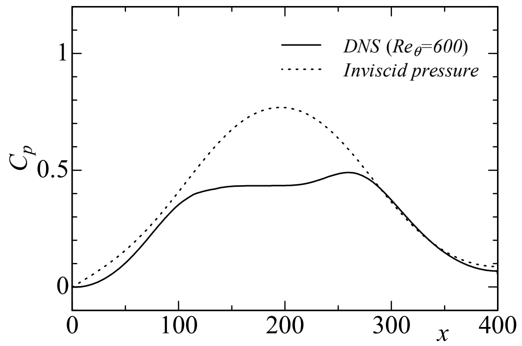

Figure 5. Distributions of C_p and the inviscid pressure.

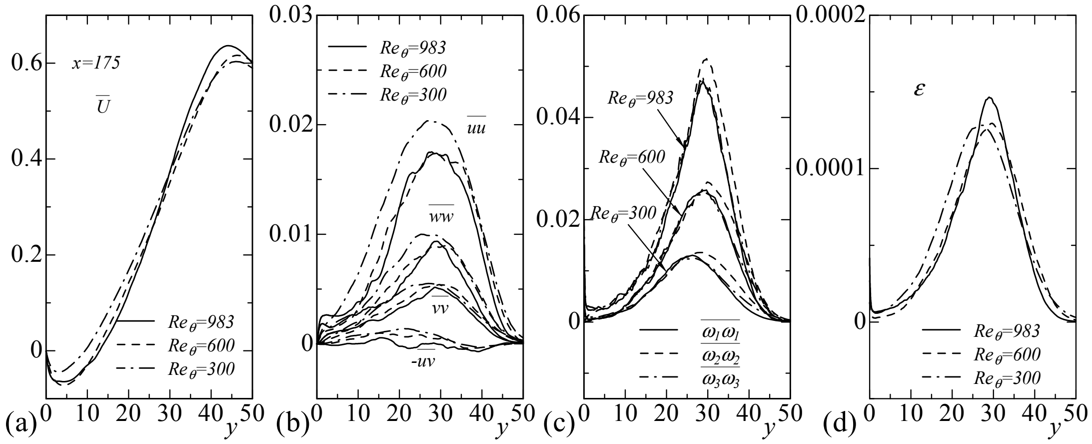

Figure 6. Distributions of mean and turbulence statistics in the separated shear layer (x=175): (a) $\overline{U}$; (b) $\overline{u_i u_j}$; (c) $\overline{\omega_i \omega_j}$; (d) ε .

RESULTS AND DISCUSSION

First, representative statistics for Re_θ = 300, such as the mean streamwise velocity $\overline{U}$ and turbulent kinetic energy k ($\equiv \overline{u_i u_i}/2$), its production P_k ($\equiv -\overline{u_i u_j} S_{ij}$) and energy dissipation rate ε ($\equiv \overline{u_{i,j}\left(u_{i,j}+u_{j,i}\right)}$), are shown in Fig. 3. Note that $S_{ij} \equiv \left(\overline{U}_{i,j}+\overline{U}_{j,i}\right)/2$; the suffixes 1,2,3 denote the streamwise, wall-normal and spanwise components, respectively; u_1,u_2,u_3 are sometimes used interchangeably with u,v,w, respectively; upper and lower cases are instantaneous and fluctuating quantities; an overbar indicates the averaging in the z direction and time.

In the separation bubble, we see clear backflow in the distribution of $\overline{U}$ (Fig. 3a), indicating massive separation. As for turbulence quantities, large magnitudes appear in the separated shear layer and reattached regions (Figs. 3b-3d). Their magnitudes are however attenuated at the top of the bubble. In particular, P_k displays a negative value, which is of course unusual, where the streamline curvature is at its most convex (Fig. 3d). An indicator of streamwise curvature $\overline{U}_{2,1}$, which comes from a rapid pressure-driven change of the mean strain rate, is associated with negative P_k. That is, the budget term arising from $\overline{U}_{2,1}$ (not shown here) yields negative Reynolds shear stress ($-\overline{u_1 u_2}$ <0) (Fig. 3e), and then the product of $-\overline{u_1 u_2}$ and $\overline{U}_{2,1}$ contributes to negative P_k. We note that these quantities are defined in the wall and wall-normal axes, which is non-unique for turbulence that is relatively far from the wall. There is also correspondence between regions with negative P_k and negative Reynolds shear stress if this stress is defined in the streamline orthogonal coordinate system, i.e.,

$$\overline{ab}=\left[\left(\overline{u_2 u_2}-\overline{u_1 u_1}\right)\overline{U}_1\overline{U}_2+\overline{u_1 u_2}\left(\overline{U}_1^{\,2}-\overline{U}_2^{\,2}\right)\right]/\left(\overline{U}_1^{\,2}+\overline{U}_2^{\,2}\right) \quad (1)$$

(Figs. 3d and f). Note a significant difference in the region 100<x<200 between $\overline{u_1 u_2}$ and $\overline{ab}$, where the streamlines are inclined at a large angle to the wall. This coordinate system is not unique either, because it is not Galilean-invariant.

Now, we focus on the Re dependence. Distributions of friction and pressure coefficients, C_f $\left(\equiv 2/U_{\infty,0}^{+2}\right)$ and $C_p\left(\equiv 2\left(P_w - P_{w,0}\right)\right)$, are given in Fig. 4 for Re_θ =300, 600 and 983 (P_w denotes the wall pressure). In the bubble, we see a decreasing magnitude of C_p with increasing Re_θ . This is interpreted as an enhanced viscid-inviscid interaction. One may also notice a plateau in the distribution of C_p for higher Re cases, indicating the presence of a dead water region. We note that there is a large difference between the inviscid pressure and C_p (Fig. 5); the latter magnitude is reduced noticeably due to the blockage by abruptly increased boundary layer thickness. By this measure, the Reynolds-number effect is small. Also, the rate of decrease of C_f with increasing Re_θ is twice as large in the recovery region as in the inlet region (see $x \approx 340$ in Fig. 4), which may be associated with weak development of near-wall turbulence in the recovery region. It can be expected that this will strongly challenge RANS models.

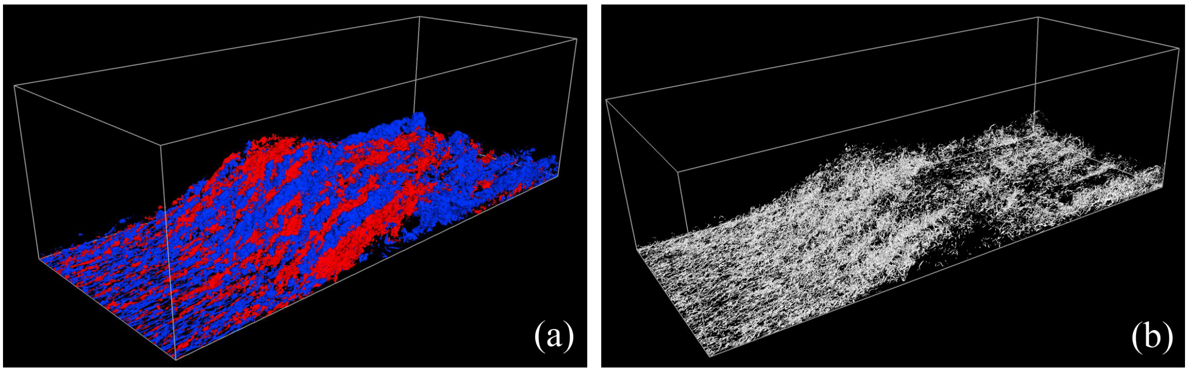

Figure 7. Isosurfaces of u and Q for Re_θ =983: (a) Red, u>0.15; blue, u<-0.15; (b) white, Q>0.01.The fluid flows from bottom-left to top-right. The visualization domain size shown here is the whole computational domain.

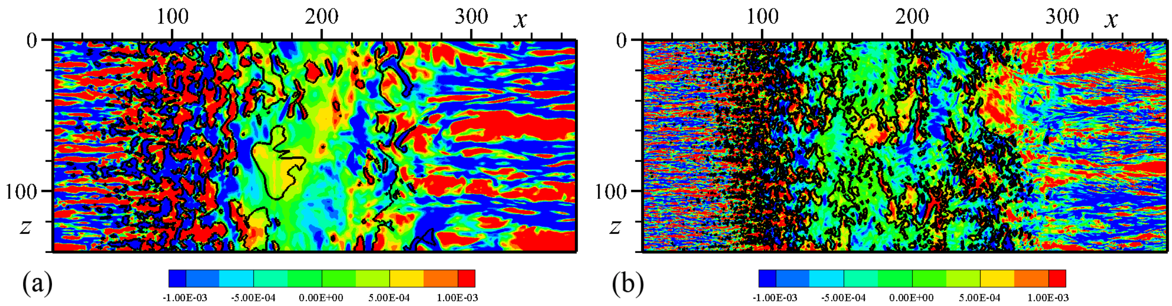

Figure 8. Contours of instantaneous $\tau_1\left(\equiv \mu\partial u/\partial y|_w\right)$ (color) and C_f (line): (a) Re_θ=300; (b) Re_θ=983. Lines denote C_f=0.

Another Re effect on statistics may be seen in the separated shear layer where the similarity to a mixing layer is sometimes discussed. The Reynolds stresses $\overline{u_iu_j}$, vorticity components $\overline{\omega_i\omega_j}$ and energy dissipation rate ε are shown in Fig. 6 together with $\bar{U}$. At this station, the maximum values of $\overline{u_iu_j}$, $\overline{\omega_i\omega_j}$ and ε appear at y=25 ~ 30 where $\bar{U}$ has its maximum gradient and hence inflection point (one exception is $-\overline{u_1u_2}$ due to the effects of streamline curvature); the Re dependence is very weak; the vorticity component is scaled reasonably after their magnitudes were normalized by the Reynolds number (i.e., a factor of 2 from Re_θ=300 to 600). This is the classical scaling for free shear flows (Bell and Mehta 1990; Rogers and Moser 1994). The maximum values normalized by the velocity difference ($\Delta\bar{U}$) also agree reasonably with those in the mixing layer, viz. $\overline{uu}/\Delta\bar{U}^2$ = 0.036 (0.025), $\overline{vv}/\Delta\bar{U}^2$ = 0.011 (0.015), $\overline{ww}/\Delta\bar{U}^2$ = 0.019 (0.020) for Re_θ =983 (numbers in parentheses are values reported by Rogers and Moser 1994), where a little larger magnitude of $\overline{uu}/\Delta\bar{U}^2$ may be associated with large-scale organized structures discussed below.

It should however be noted that the classical mixing layer-like structure with large quasi-two-dimensional rollers is not observed in the instantaneous field (see Fig. 7 which shows isosurfaces of instantaneous u and $Q\left(\equiv -u_{i,j}u_{j,i}/2\right)$ for Re_θ =983). Instead, there are large-scale positive and negative u structures appearing alternatively in the z direction (Fig. 7a) at high Re (see also a dense clustering of vortical structures in Fig. 7b). Also, the structures are more significant in the reattached region than in the shear layer (Fig. 7) probably due to effects of inflectional instabilities coming from the shear layer. There are also footprints of large-scale structures onto the wall, i.e., large-scale meandering of the separation lines, large-scale fluctuations in the separated region and dense clustering of streaky structures in the reattached region (see Fig. 8b). The apparent streak spacing is, naturally, smaller at the higher Reynolds number after the normalization by θ_0 (Fig. 8).

Finally, we turn our attention to turbulence model testing. Three models, namely k-ε (Abe et al. 1994), k-ω (Wilcox 1988) and SST (Menter 1994) are examined. The inlet data are provided by the DNS data. We emphasize that we match the inflow eddy viscosity ν_t, rather than the specific dissipation rate (or turbulence frequency) ω for the k-ω and SST models. Note that in the k-ε model, prescription of ε from k and ν_t($\equiv 0.09 f_\mu k^2/\varepsilon$) is not straightforward due to the presence of near-wall damping function f_μ so that k and ε are used. Indeed, the use of k and ν_t as the inflow conditions is effective for having a smooth C_f distribution near the inlet region (see Fig. 9a). The same grid is used as for DNS, in the (x,y) plane, which allows us to make direct comparisons between DNS and RANS results readily.

The representative results are shown in Figs. 9-11. Overall, the k-ε model gives the best prediction among the three models. The present result may not be surprising given that this model predicts the backward facing step reasonably. The k-ω and SST models tend to show a larger separation bubble than the k-ε model (Fig. 10). Note that the prediction is improved for a high Re case (the results are not shown here). One may notice that in

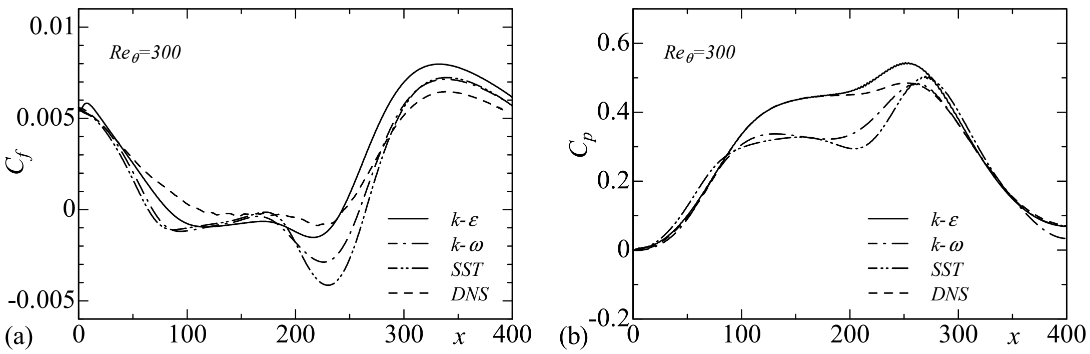

Figure 9. Model performance for C_f and C_p at Re_θ=300: (a) C_f; (b) C_p.

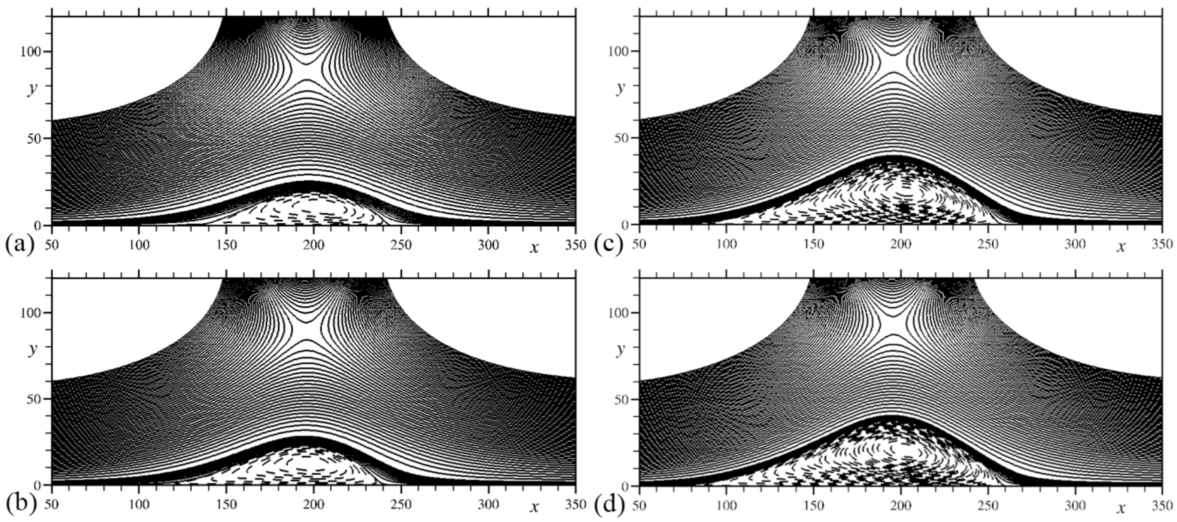

Figure 10. Model performance for streamlines at Re_θ =300: (a) DNS; (b) k-ε ; (c) k-ω ; (d) SST. Solid and dashed lines denote positive and negative streamlines.

the k-ω model a noticeable surge of the turbulent eddy viscosity ν_t appears close to the upper boundary (Fig. 11). This is due to the presence of large velocity gradient close to the upper boundary, which leads to significant disturbances in the k-ω model. The limiter min(P_k, 10ε) for both k and ω equations in the SST model avoids this disturbance successfully. In Fig. 11a, an effective eddy viscosity, $\nu_t \equiv -\overline{u_i u_j} S_{ij} / 2S_{kl}S_{kl}$, is proposed from the DNS, which can be described as a least-squares fit to the Reynolds-stress tensor, or as the scalar eddy viscosity which provides the correct production. As a result, it takes negative values in the region of negative P_k (see Fig. 3d); RANS models are certainly not expected to follow such behavior (Figs. 11b-d).

Also, in the negative ν_t region, we see rapid re-orientation of the strain eigenvector, while the direction of the stress eigenvector changes slowly (see misalignment between the two eigenvectors in Fig. 11a), which is another interpretation for negative P_k (note that P_k is described as the product of strain and stress tensors, so that P_k becomes negative when their directions are more than 45° different).

This approach to exploiting DNS fields is not wide-spread, but appears to have potential. For instance, the eddy viscosity of the models is much smaller than that of the DNS over large areas, but this short separation bubble may be dominated by the inviscid transport of vorticity, so that the velocity does not respond rapidly to inaccuracies in the modeling.

CONCLUSIONS

In the present study, we have performed DNSs of a turbulent boundary layer with separation and reattachment for inflow Re_θ =300, 600 and 983. Also reported are results regarding two-equation model testing made using the resulting DNS data. The main conclusions are:

(1) The effects of streamline curvature are strong in the bubble. In particular, the magnitudes of turbulence quantities are attenuated at the top of the bubble, which can be attributed to the convex curvature, or to the rapid re-orientation of the principal axes of the strain tensor.

(2) The Re effects on statistics are a mild decrease of C_p in the bubble with increasing Re_θ. In the shear layer, free-shear-flow scaling appears to be applicable to a good degree statistically, both for the Reynolds stresses and the dissipation. The same is however not true of the small eddies in the instantaneous field. In addition, the recovery after reattachment has a strong Reynolds-number dependence.

(3) At high Re, there are large-scale organized u structures in the separated and reattached regions. There are also their footprints onto the wall, viz., large-scale

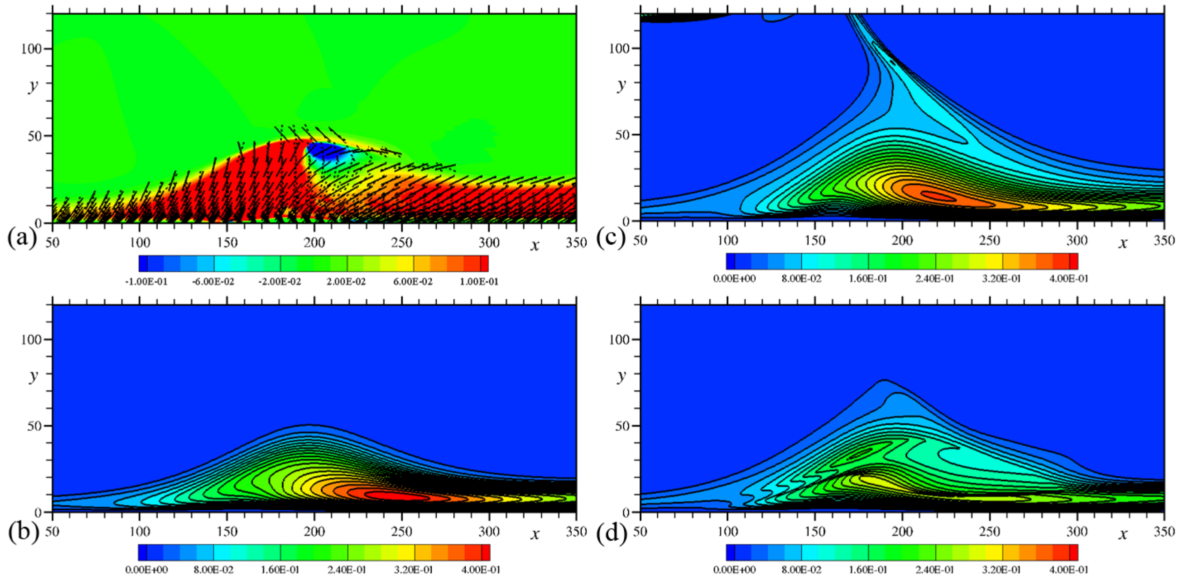

Figure 11. Model performance for ν_t at Re_θ=300: (a) DNS; (b) k-ε; (c) k-ω; (d) SST. In (a), solid and dashed lines denote eigenvectors (associated with the positive eigenvalue) of S_{ij} and $-\overline{u_i u_j}$, respectively. Note the definition in DNS, $\nu_t \equiv -\overline{u_i u_j} S_{ij} / 2 S_{kl} S_{kl}$, which is a coordinate-invariant form.

meandering of the separation lines, large-scale fluctuations in the separated region and dense clustering of streaky structures in the reattached region.

(4) The k-ε (Abe et al. 1994) model gives the best prediction among the three models, which is a little unusual; the k-ω (Wilcox 1988) and SST (Menter 1994) models show a larger separation bubble than the k-ε model.

(5) A troublesome freestream sensitivity appears in the k-ω model due to the presence of large velocity gradients close to the upper boundary. The limiter min(P_k, 10ε) in the SST model avoids this shortcoming successfully.

ACKNOWLEDGEMENTS

Computations performed on JAXA (Japan Aerospace Exploration Agency) Supercomputer System are gratefully acknowledged.

REFERENCES

Abe, H., Kawamura, H. and Matsuo, Y., 2004, "Surface Heat-Flux Fluctuations in a Turbulent Channel Flow up to Re_τ =1020 with Pr=0.025 and 0.71," *Int. J. Heat and Fluid Flow*, Vol. 25, pp. 404–419.

Abe, K., Kondoh, T. and Nagano, Y., 1994, "A New Turbulence Model for Predicting Fluid Flow and Heat Transfer in Separating and Reattaching Flows-l. Flow field calculations," *Int. J. Heat Mass Transfer*, Vol. 37, pp. 139–151.

Bell, J. H. and Mehta, R. D., 1990, "Development of a Two-Stream Mixing Layer from Tripped and Untripped Boundary Layers," *AIAA J.*, Vol. 28(12), pp. 2034–2042.

Leschziner, M.A., 2006, "Modelling Turbulent Separated Flow in the Context of Aerodynamic Applications," *Fluid Dyn. Res.*, Vol. 38, pp. 174–210.

Lund, T.S., Wu, X. and Squires, K.D., 1998, "Generation of Turbulent Inflow Data for Spatially-Developing Boundary Layer Simulation," *J. Comput. Phys.*, Vol. 140, pp. 233–258.

Manhart, M. and Friedrich, R., 2002, "DNS of a Turbulent Boundary Layer with Separation," *Int. J. Heat and Fluid Flow*, Vol. 23 , pp. 572–581.

Menter, F. R., 1994, "Two-Equation Eddy-Viscosity Turbulence Models for Engineering Applications," *AIAA J.*, Vol. 8, pp. 1598–1605.

Morinishi, Y., Lund, T. S., Vasilyev, O. V. and Moin, P., 1998, "Fully Conservative Higher Order Finite Difference Schemes for Incompressible Flow.," *J. Comput. Phys.*, Vol. 143(1), pp. 90–124.

Purtell, L. P., Klebanoff, P. S. and Buckley, F. T., 1981, "Turbulent Boundary Layer at Low Reynolds number," *Phys. Fluids*, Vol. 24(5), pp. 802–811.

Rogers, M. M. and Moser, R. D., 1994, "Direct Simulation of a Self-Similar Turbulent Mixing Layer," *Phys. Fluids*, Vol. 8(2), pp. 903–923.

Skote, M. and Henningson, D.S., 2002, "Direct Numerical Simulation of a Separated Turbulent Boundary Layer," *J. Fluid Mech.*, Vol. 471, pp. 107–136.

Simpson, R.L., 1989, "Turbulent Boundary-Layer Separation," *Ann. Rev. Fluid Mech.*, Vol. 21, pp. 205–234.

Song, S. and Eaton, J. K., 2004, "Reynolds Number Effects on a Turbulent Boundary Layer with Separation, Reattachment, and Recovery," *Exp. Fluids*, Vol. 36, pp. 246–258.

Spalart, P.R. and Coleman, G.N., 1997, "Numerical Study of a Separation Bubble with Heat Transfer," *Eur. J. Mech. B/Fluids*, Vol. 16, pp. 169–189.

Wilcox, D.C., 1988, "Reassessment of the Scale-Determining Equation for Advanced Turbulence Models," *AIAA J.*, Vol. 26, pp. 1299–1310.